Yield stress fluid behavior of foam in porous media

Alexis Mauray,[1] Max Chabert,[2] and Hugues Bodiguel[1,*]
[1]*Université Grenoble Alpes, CNRS, Grenoble-INP, LRP UMR 5520, F-38000 Grenoble, France*
[2]*Solvay, 1 Biopolis Drive, 138622 Singapore*

(Received 11 June 2019; accepted 17 July 2020; published 17 September 2020)

Flow of foams is studied in a model porous medium, in a large range of capillary numbers Ca and relative gas flow rates f_g. From pressure measurements, we find that the effective viscosity is a decreasing power-law function of Ca, with the exponent ranging from -1 to -0.75. Direct observation reveals that the flow is heterogeneous. The fraction of preferential paths increases with both f_g and Ca. In a straight channel of varying cross section, a bubble train behaves as a shear-thinning yield stress fluid. This feature accounts quantitatively for the effective viscosity in the micromodel.

DOI: 10.1103/PhysRevFluids.5.094004

I. INTRODUCTION

Many industrial processes involve gas-liquid flows through porous media. Prominent examples can be found in petroleum [1] and in chemical engineering [2]. Some take advantage of the addition of surfactants to stabilize the gas-liquid interfaces, leading to the formation of foam in earth's subsurface flows, in particular to enhance oil recovery or to clean polluted soils [3]. Injecting foams into rocks presents numerous advantages as the needed volumes of water are considerably lowered and as the specific rheological properties of the foam allow better invasion into small pores [4]. Because of its high effective viscosity, foam also reduces both channeling flows (flows of gas in the high-permeability streaks) and viscous fingering. In this context, understanding physical mechanisms behind foam flow behavior in porous media has been the subject of many studies and still holds open questions today.

Most experimental studies focused on macroscopic flows of foam in realistic porous materials such as packed grains and porous solids [5–8]. Although these studies provide important insights, flow at the level of the pore cannot be accessed, and they yield only a limited microscopic description of the mechanisms ruling foam flows in porous media. One of the major difficulties originates from the multiple physical mechanisms at work [4] (foam formation and lamella division, coalescence, transport, channeling, buoyancy effects, wetting properties, etc.) and the multiple parameters involved, usually not accessible experimentally in real rocks.

Therefore, two-dimensional micromodels have been used for a few decades to better understand the relevant mechanisms in two-phase flows in porous media [9–11]. Such devices have been used in the past few years to visualize foam flows in heterogeneous media [12–16] but have not yet been applied to quantitatively characterize the most important parameter of foam from the application standpoint, i.e., its effective viscosity in porous media. Bubble and droplet traffic has been extensively studied and is rather well understood in the dilute limit pertaining to applications in digital microfluidics [17–23], but these studies focus on too simple geometries or on too dilute regimes to be directly extended to porous media.

*hugues.bodiguel@univ-grenoble-alpes.fr

Foam rheology in porous media totally differs from that evaluated in bulk measurements, with generally higher viscosities linked to confinement of foam bubbles in pore space [4]. It exhibits two regimes macroscopically, depending on the relative gas flow rate $f_g = Q_g/(Q_g + Q_l)$, where Q_g and Q_l are the gas and liquid flow rates, respectively [7,24]. Below $f_g \sim 0.8$ (the so-called low-quality regime), it increases when f_g is increased, whereas at higher f_g, it decreases due to lamella coalescence [25]. In the low-quality regime, on which we focus here, recent experimental results revealed that the foam is strongly shear thinning; its viscosity scales as Ca^{-n}, with n ranging from 0.6 to 0.9 [26,27] and Ca being the capillary number, defined as $\mathrm{Ca} = \mu V/\gamma$, where μ is the water viscosity, V is the velocity, and γ is the surface tension. The high effective viscosity is usually described in mechanistic models as the combination of two mechanisms [4,28]. First, the motion of the dispersed gas phase involves dynamic menisci [22,29], as theoretically studied by Bretherton [30], which induces extra dissipation that scales as $\mathrm{Ca}^{2/3}$. Second, as inferred [4,31] and experimentally demonstrated [8,14,15], only a fraction of the gas contributes to the flow in preferential paths, while the other fraction remains trapped. Intuitively, it is tempting to attribute the strong shear thinning behavior to the combination of the two mechanisms. We experimentally demonstrate here that none of them are relevant.

We consider in this work foam flow in a heterogeneous two-dimensional (2D) porous medium with well-controlled geometry. The key experimental results are obtained by combining pressure measurements and direct observations, varying both gas and liquid flow rates in a very large range, in the low-Reynolds-number regime. We observe the generic behavior and foam effective viscosity values that were reported in three-dimensional (3D) porous media, in the low-quality regime. In particular, we find that the effective viscosity scales as a power law of the capillary number: Ca^{-n}, with n between 0.7 and 0.9. In contrast, unexpectedly, the number of preferential paths exhibits a weak dependency on Ca, ruling out their impact on foam shear-thinning behavior. We then report results from further experiments prompted by this finding. In a single channel of varying cross section, we evidence a deviation from Bretherton's law at low Ca. Using this result, we are able to account quantitatively for the effective viscosity measured in the micromodel.

II. EXPERIMENTAL METHODS

The device used in this study is a microfluidic chip made in optical glue [32,33] consisting of an $L \times W = 3 \times 2$ cm^2 2D random porous medium [34], obtained using a simple numerical algorithm (see the Supplemental Material for details [35], Sec. I B) and displayed in Fig. 1 (top left panel). The height h of the device is 180 μm. The correlation length of the porous medium is set to $l_c = 200\,\mu$m; its 2D porosity ϕ is set to 0.7. The pore size exhibits a mean value of $\langle w \rangle = 134\,\mu$m, while the mean pore throat diameter is about 95 μm [36]. Its permeability has been determined experimentally, $k = 9.25 \times 10^{-11}$m^2 (see the Supplemental Material for details [35], Sec. I C).

The flow is controlled using a syringe pump (Nemesys), and the outlet is connected to a pressurized reservoir, set at 3 bars to allow neglecting the impact of gas compressibility. A differential pressure sensor is used between the inlet and the outlet to determine the pressure drop. The experimental setup is complemented by a fast camera (Mikrotron) mounted on an optical lens (Nikon). All experiments are carried out with an aqueous solution of 5% in weight of Solvay SurfEOR surfactant, which allows avoiding bubble coalescence and ensures total wetting, a typical situation in real rocks. The surface tension γ of the solution is 33 mN m^{-1}, as determined using the pendant drop method.

The gas-liquid coinjection protocol has been carefully established to avoid entrance effects and to dissociate foam formation from its steady-state flow properties. We proceed as follows: first, we generate big bubbles by using a T junction connected to two syringes, controlled at flow rates of Q_g and Q_l, for the gas and liquid phases, respectively. When entering the porous medium, these bubbles progressively divide, provided that the total flow rate is high enough. Eventually, they reach a size which is similar to that of the pore size, so that division mechanisms are subsequently inefficient [14,37]. Then, in order to ensure a steady state, we collect the effluents and reinject

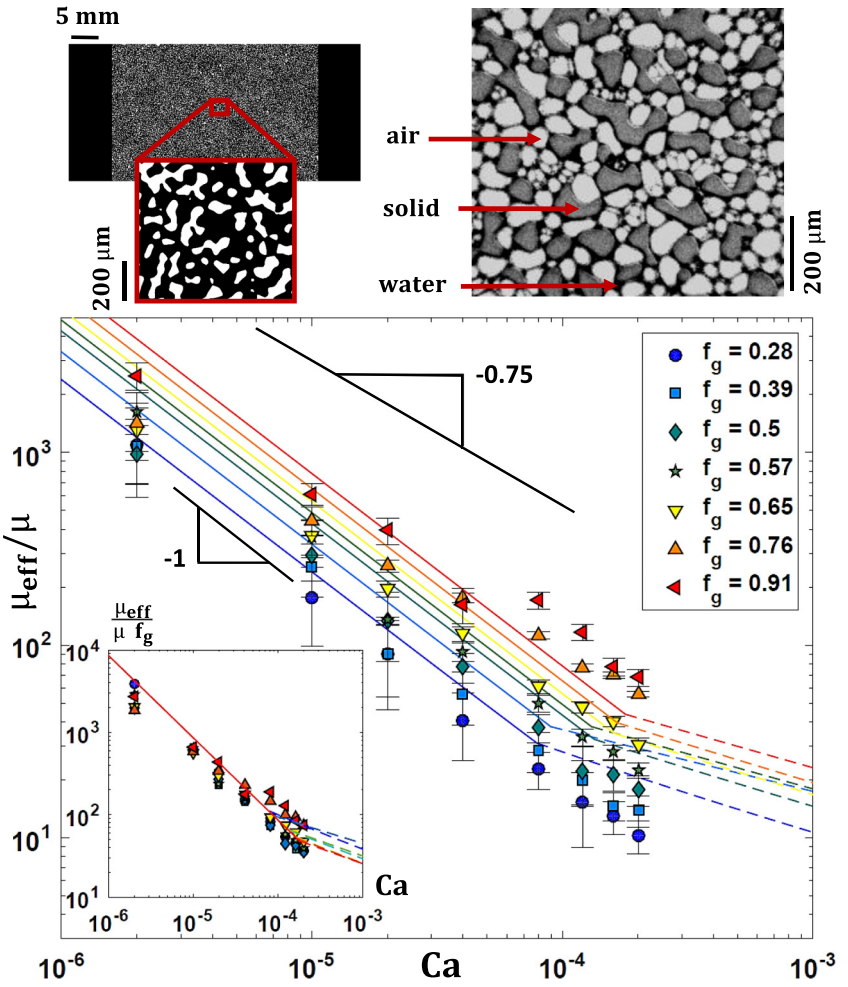

FIG. 1. Top: images of the mask used to fabricate the device and a magnified image taken during foam flow. Bottom: Relative foam effective viscosity μ_{eff}/μ as a function of Ca for various f_g. Lines correspond to the semiempiric predictions (see text): solid ones for the threshold regime, and dashed ones for the Bretherton regime.

them into the porous domain once again at high flow rate. In this second step, we observe that the mean bubble size remains constant. We thus obtain a so-called strong foam [38] which consists of bubbles of about the pore size, generated by the porous medium itself. This foam is finally injected at a desired flow rate, which is generally much lower. By construction, the relative gas flow rate $f_g = Q_g/(Q_g + Q_l)$ is controlled by the first generation step. This protocol ensures that the injected phases have the same texture whatever the value of Ca. In the following, the capillary number is precisely defined as $\text{Ca} = \mu(Q_l + Q_g)/\gamma\phi hW$, where μ is the aqueous solution viscosity] $(1 \pm 0.08) \times 10^{-3}$ Pa s].

III. RESULTS

A. Foam effective viscosity measurement in the model porous medium

Figure 1 (bottom) summarizes the main result of this work. It displays the relative effective viscosity μ_{eff}/μ, corresponding to the measured pressure drop ΔP in the presence of bubbles

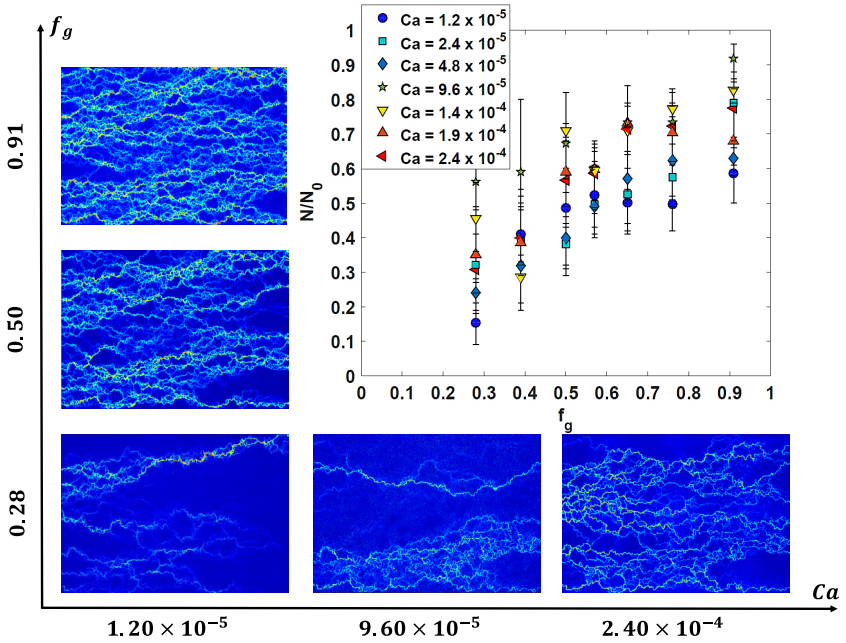

FIG. 2. Examples of time-averaged image differences highlighting preferential paths. In the inset, the fraction of these paths, N/N_0, is plotted as a function of Ca for various relative gas flow rates f_g.

normalized by the pressure drop ΔP° due to water flowing at the same total flow rate. This definition of the effective viscosity implicitly assumes a generalized Darcy's law, commonly used for monophasic non-Newtonian fluids, with the capillary number being a normalized shear rate. For every f_g tested, the effective viscosity decreases when the capillary number is increased and follows a power law with the exponent ranging between -1 for the lowest f_g tested and -0.75 for the highest one. When f_g is increased, the effective viscosity increases as well. Let us highlight that the very high values of the relative effective viscosity reached at low Ca (more than 2000!) correspond to orders of magnitude reported for foams flows in real rocks [5]. Furthermore, the power-law behavior with respect to Ca is similar to that in real porous media [25–27]. Thus, these model experiments contain the minimal physical ingredients for describing effective viscosity in foam flow in porous media.

B. Study of the preferential paths

The movies acquired together with the pressure measurements reveal that the flow is heterogeneous (see, for example, the movies available in the Supplemental Material [35]): in some regions of the porous domain, gas bubbles are trapped and do not contribute to the flow. The latter is concentrated in preferential paths. In order to characterize these, we compute the absolute difference between successive images and average in time (see the Supplemental Material for details [35]). Examples are displayed in Fig. 2, and the complete data set is available in the Supplemental Material [35]. These images highlight qualitatively the preferential paths. One can notice that their number slightly increases when increasing Ca and also when increasing f_g. More quantitatively, we estimate the fraction of the pores that contributes to the flow by computing the mean value of the binary image obtained after thresholding. This fraction is defined hereafter as the ratio of effective flowing paths N over the number of available ones N_0. The results are displayed in Fig. 2. For a given f_g, N/N_0 does not greatly vary when varying Ca. On the contrary, this ratio strongly depends on f_g. Strikingly, the higher f_g is, the more homogeneous the flow is.

Since we know precisely the characteristics of the porous medium and we get an estimate of the ratio of preferential paths, we now try to discuss more quantitatively the mobility reduction values. The simplest model to test consists of a bundle of N parallel channels, in which bubble trains are flowing. Dedicated microfluidic studies [22] on bubble trains have verified that Bretherton's law [30] applies, even for dense bubble trains. Each bubble creates an extra pressure drop proportional to $p_c \mathrm{Ca}_l^{2/3}$, where p_c is the mean capillary pressure, set by the channel geometry, $p_c = 2\gamma(1/h + 1/\langle w \rangle)$, and Ca_l is the local capillary number. Since only a fraction N/N_0 of the medium contributes to the flow, local velocities are greater by a factor of N_0/N than the pore velocity estimated for a mean homogeneous flow, i.e., $\mathrm{Ca}_l = \mathrm{Ca} N_0/N$. Neglecting the other contributions to the total pressure drop, which is justified by the high values of the mobility reduction, we expect that the latter would be proportional to $\mathrm{Ca}^{-1/3}(N_0/N)^{2/3}$ since ΔP_0 is proportional to Ca. However, as the fraction of preferential paths shows only a weak dependence on Ca, the above model cannot account for the strong shear thinning found experimentally. We conclude that Bretherton's law in straight channels cannot be directly extrapolated to the tortuous flow paths in the porous medium, although that is a common assumption in mechanistic models [6,29,39,40].

C. Flow of a train of bubbles in two different geometries of a single channel

In order to get deeper insights into the mechanisms responsible for the effective viscosity, we performed similar experiments in two much simpler geometries, which consist of a single channel, either with a uniform cross section or with a sinusoidal cross section. In the second case, our intention is to mimic the succession of constrictions during bubble motion in the porous medium [41–43]. The geometric features of this device (width and height, amplitude, and wavelength of the sine function) are close to those of the pores in the micromodel. Details are given in the Supplemental Material [35]. Using a flow-focusing element [44], we inject a periodic train of monodisperse bubbles in these channels. The bubble size is slightly larger than the mean width. We systematically measure the pressure drop as a function of the two parameters of the problem: the wavelength of the bubble train and the capillary number.

We aim at measuring the extra pressure drop due to a single bubble ΔP_b. For that purpose, we substract from the total pressure the contribution of the continuous phase in between the bubbles, assuming Poiseuille's law, and then divide it by the number of bubbles in the channels estimated knowing the wavelength of the bubble train [19,22]. The results are displayed in Fig. 3. For both channels, all the data collapse when plotted as a function of Ca. This shows that the bubble density has no direct influence on pressure drop *per* bubble, although the total pressure drop depends on the bubble wavelength. For the channel with a uniform cross section, the data are rather well accounted for by Bretherton's law, $\Delta P_b = \alpha p_c \mathrm{Ca}^{2/3}$. The empiric prefactor α is quite high—and different from the theoretical prediction of Bretherton—since we find $\alpha = 17$. This deviation is similar to previously reported data [19,22] and might be associated with the impact of the surfactant and could thus depend on its interfacial properties. For the channel with a sinusoidal cross section, we find a very different behavior. Two regimes are evidenced around a threshold capillary number $\mathrm{Ca}_c = 2.3 \times 10^{-4}$. For $\mathrm{Ca} > \mathrm{Ca}_c$, we recover a Bretherton-like law, with $\alpha \simeq 35$. At lower capillary numbers, data deviate from this law, and the bubble pressure drop exhibits a plateau, around $\beta\langle p_c \rangle$, where $\beta \simeq 0.13$. The motion of a bubble train in a channel with constrictions is thus similar to that of a yield stress fluid: there is a pressure threshold below which a bubble does not flow, and its value is a fraction of the capillary pressure. In the following, we refer to these two regimes as the *threshold regime* and the *Bretherton regime*.

IV. DISCUSSION

Since the geometrical features of the channel with a sinusoidal cross section are very similar to the ones of the porous media, we may use quantitatively the results obtained in the channel and

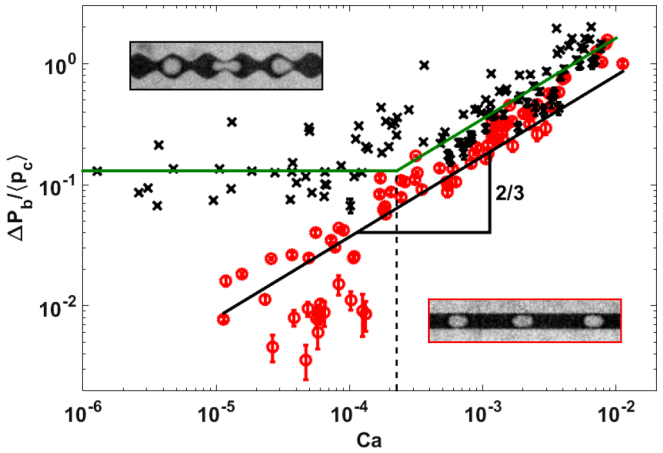

FIG. 3. Pressure drop induced by a single bubble ΔP_b, normalized by the capillary pressure $\langle p_c \rangle = 2\gamma(1/h + 1/\langle w \rangle)$ as a function of Ca, in two geometries: a channel of uniform cross section (red circles) and a channel of sinusoidal width (black crosses). Data correspond to various wavelengths, so that this parameter appears to be irrelevant. Solid lines represent the best fit to the data. For the uniform-cross-section case, we find a Bretherton law $\alpha \mathrm{Ca}^{2/3}$, with $\alpha = 17$. For the varying-cross-section case, we find $\beta = 35$ in the Bretherton regime (for $\mathrm{Ca} > 2.3 \times 10^{-4}$) and $\beta = 0.13$ in the threshold regime.

extrapolate to the porous medium case. By estimating the number of bubbles involved in one of the preferential paths, we obtain (see the Supplemental Material for details [35]) that, in the threshold regime, $\Delta P/\Delta P_0 = a\beta f_g \mathrm{Ca}^{-1}$, where the geometric constant $a \simeq 0.066$ [35,45]. When the local capillary number exceeds Ca_c, i.e., for $\mathrm{Ca}N_0/N > \mathrm{Ca}_c$, the Bretherton regime should hold, and we expect that $\Delta P/\Delta P_0 = a\alpha f_g (N_0/N)^{2/3} \mathrm{Ca}^{-1/3}$.

The two regimes are plotted in Fig. 1. It turns out that most experiments fall in the threshold regime; only the highest tested flow rate is in the Bretherton regime. Thus, the present set of data does not evidence the transition. Nevertheless, the above semiempiric predictions account rather nicely for the effective viscosity data, although they slightly overestimate the effective viscosity at high f_g and low Ca and underestimate the power-law exponent at high f_g. We can thus infer that the threshold regime also occurs in the porous medium and that it is responsible for the strong apparent shear-thinning effect which is measured. Strikingly, the number of preferential paths has no direct effect on the effective viscosity in this regime and influences only the onset of the Bretherton regime.

Eventually, it is worth discussing the physical mechanisms underlying the threshold regime. Such a threshold has been predicted theoretically [46]. It originates from a coupling between the meniscus motion and the capillary pressure difference that appears between the front and rear menisci of a bubble passing a constriction. Although this pressure difference is symmetric with respect to the bubble position, the fact that a bubble moves slower upstream than downstream of the constriction leads, after averaging over time and space, to a net pressure drop. It is of the order of a fraction of $\langle p_c \rangle$, as observed in our experiments. To verify this mechanism, we perform image analysis on the movie acquired in the straight channel with a varying cross section and estimate the curvature difference between the front and rear menisci of single bubbles. As shown in Fig. 4, we find that it fluctuates in correspondence to bubble displacement through successive constrictions. Bubble motion is nonsteady, and the bubble spends more time upstream of the constriction, where the pressure difference between the front and rear menisci is positive, rather than downstream, where it is negative. As a result, the pressure mean value is nonzero and in qualitative agreement with the value of $\beta = 0.13$ obtained from the pressure drop measurement.

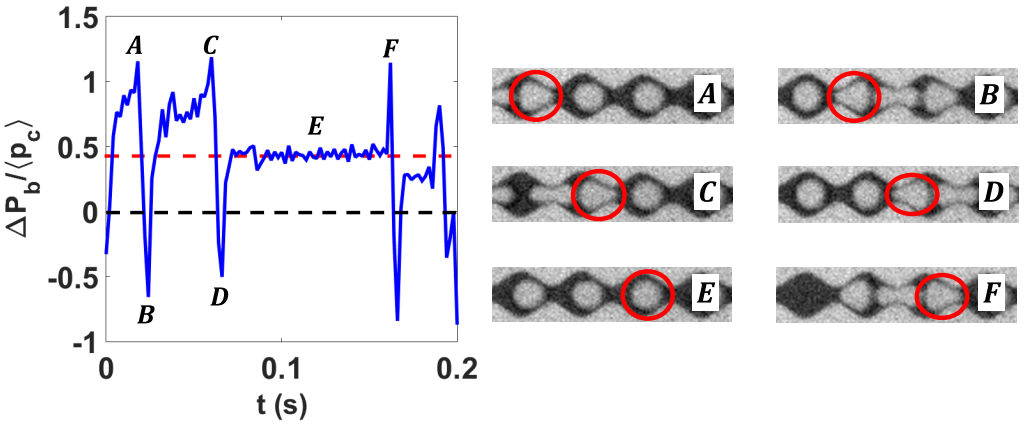

FIG. 4. Example of normalized instantaneous pressure difference per bubble as a function of time, as determined by the estimation of the menisci curvature on the images. In this experiment, Ca $= 10^{-5}$. In the six images labeled from A to F, the bubble of interest is highlighted in red. The times corresponding to these six images are displayed on the plot. The dashed line represents the mean value.

V. CONCLUDING REMARKS

In summary, we reported in this paper a complete data set of foam effective viscosities in the low-quality regime, acquired in a bidimensional transparent porous medium. We evidenced, as in real rocks, high values of effective viscosity and a strongly shear thinning behavior. Direct observation revealed that the flow is heterogeneous and concentrated in some preferential paths. Interestingly, the flow becomes more homogeneous when the bubble density is high. This result has strong practical consequences since foam is generally used (either in oil recovery or in soil remediation) to better sweep porous media and the most homogeneous flow is interesting for that purpose. Contradicting an usual paradigm, we showed that variation in the number of preferential paths with capillary number is irrelevant to adequately describe foam rheology in porous media. Indeed, using model experiments in a simple channel of varying cross section, we evidenced that, at the low capillary numbers investigated, the pressure drop per bubble actually becomes independent of the flow rate and is simply a fraction of the capillary pressure. Extrapolation of this result to the porous medium allows, without additional significant assumptions, capturing reasonably well the measured values of the effective viscosity in a large range of Ca and f_g. Foam flow at larger scale in 3D porous media would, however, require us to incorporate buoyancy effects, permeability heterogeneities, foam stability issues, etc. In addition, some features of the problem still remain to be investigated. We observed, but did not analyze in detail, that the motion of the bubbles is locally not steady but intermittent at high bubble densities, even though the flow appears to be rather continuous when averaged over time. The variation of the shear-thinning exponent, from 1 at low f_g to about 0.75 at high f_g, is currently not captured by the model and calls for refinements and additional work. It would also be interesting to increase further the capillary number in order to confirm the existence of a Bretherton-like regime above Ca_c.

ACKNOWLEDGMENTS

The authors acknowledge Solvay for financial support. LRP is a part of the LabEx Tec 21 (Investissements d'Avenir, Grant Agreement No. ANR-11-LABX-0030) and PolyNat Carnot Institute (Grant Agreement No. ANR-11-CARN-030-01).

[1] L. W. Lake, *Enhanced Oil Recovery* (Prentice Hall, Englewood Cliffs, 1989).
[2] M. H. Al-Dahhan, F. Larachi, M. P. Dudukovic, and A. Laurent, High-pressure trickle-bed reactors: A review, Ind. Eng. Chem. Res. **36**, 3292 (1997).
[3] C. N. Mulligan, R. N. Yong, and B. F. Gibbs, Remediation technologies for metal-contaminated soils and groundwater: An evaluation, Eng. Geol. **60**, 193 (2001).
[4] A. R. Kovscek and C. J. Radke, *Fundamentals of Foam Transport in Porous Media*, in Foams: Fundamentals and Applications in the Petroleum Industry, Advances in Chemistry Vol. 242 (American Chemical Society, Washington, DC, 1994), p. 115.
[5] Z. I. Khatib, G. J. Hirasaki, and A. H. Falls, Effects of capillary pressure on coalescence and phase mobilities in foams flowing through porous media, SPE Reserv. Eng. **3**, 15442 (1988).
[6] A. R. Kovscek and H. J. Bertin, Foam mobility in heterogeneous porous media, Transp. Porous Media **52**, 17 (2003).
[7] J. M. Alvarez, H. J. Rivas, and W. R. Rossen, Unified model for steady-state foam behavior at high and low foam qualities, SPE J. **6**, 325 (2001).
[8] G.-Q. Tang and A. R. Kovscek, Trapped gas fraction during steady-state foam flow, Transp. Porous Media **65**, 287 (2006).
[9] R. Lenormand and C. Zarcone, Invasion Percolation in an Etched Network: Measurement of a Fractal Dimension, Phys. Rev. Lett. **54**, 2226 (1985).
[10] O. I. Frette, K. J. Maløy, J. Schmittbuhl, and A. Hansen, Immiscible displacement of viscosity matched fluids in two-dimensional porous media, Phys. Rev. E **55**, 2969 (1997).
[11] C. Cottin, H. Bodiguel, and A. Colin, Drainage in two-dimensional porous media: From capillary fingering to viscous flow, Phys. Rev. E **82**, 046315 (2010).
[12] K. Ma, R. Liontas, C. A. Conn, G. J. Hirasaki, and S. L. Biswal, Visualization of improved sweep with foam in heterogeneous porous media using microfluidics, Soft Matter **8**, 10669 (2012).
[13] C. A. Conn, K. Ma, G. J. Hirasaki, and S. L. Biswal, Visualizing oil displacement with foam in a microfluidic device with permeability contrast, Lab Chip **14**, 3968 (2014).
[14] J. Gauteplass, K. Chaudhary, A. R. Kovscek, and M. A. Fernø, Pore-level foam generation and flow for mobility control in fractured system, Colloids Surf. A **468**, 184 (2015).
[15] B. Géraud, S. A. Jones, I. Cantat, B. Dollet, and Y. Méheust, The flow of a foam in a two-dimensional porous medium, Water Resour. Res. **52**, 773 (2016).
[16] B. Géraud, Y. Méheust, I. Cantat, and B. Dollet, Lamella Division in a Foam Flowing through a Two-Dimensional Porous Medium: A Model Fragmentation Process, Phys. Rev. Lett. **118**, 098003 (2017).
[17] W. Engl, M. Roche, A. Colin, P. Panizza, and A. Ajdari, Droplet Traffic at a Simple Junction at Low Capillary Numbers, Phys. Rev. Lett. **95**, 208304 (2005).
[18] W. Choi, M. Hashimoto, A. K. Ellerbee, X. Chen, K. J. M. Bishop, P. Garstecki, H. A. Stone, and G. M. Whitesides, Bubbles navigating through networks of microchannels, Lab Chip **11**, 3970 (2011).
[19] M. J. Fuerstman, A. Lai, M. E. Thurlow, S. S. Shevkoplyas, H. A. Stone, and G. M. Whitesides, The pressure drop along rectangular microchannels containing bubbles, Lab Chip **7**, 1479 (2007).
[20] P. Parthiban and S. A. Khan, Bistability in droplet traffic at asymmetric microfluidic junctions, Biomicrofluidics **7**, 044123 (2013).
[21] N. Champagne, R. Vasseur, A. Montourcy, and D. Bartolo, Traffic Jams and Intermittent Flows in Microfluidic Networks, Phys. Rev. Lett. **105**, 044502 (2010).
[22] V. Hourtane, H. Bodiguel, and A. Colin, Dense bubble traffic in microfluidic loops: Selection rules and clogging, Phys. Rev. E **93**, 032607 (2016).
[23] H. Wong, C. J. Radke, and S. Morris, The motion of long bubbles in polygonal capillaries. Part 1. Thin films, J. Fluid Mech. **292**, 95 (1995).
[24] W. T. Osterloh and M. J. Jante, Jr., *Effects of Gas and Liquid Velocity on Steady-State Foam Flow at High Temperature* (Society of Petroleum Engineers, 1992).
[25] M. Lotfollahi, R. Farajzadeh, M. Delshad, A. Varavei, and W. R. Rossen, Comparison of implicit-texture and population-balance foam models, J. Nat. Gas Sci. Eng. **31**, 184 (2016).
[26] O. Gassara, F. Douarche, B. Braconnier, and B. Bourbiaux, Calibrating and interpreting implicit-texture models of foam flow through porous media of different permeabilities, J. Pet. Sci. Eng. **159**, 588 (2017).

[27] S. A. Jones, N. Getrouw, and S. Vincent-Bonnieu, Foam flow in a model porous medium: II. The effect of trapped gas, Soft Matter **14**, 3497 (2018).
[28] H. Hematpur, S. M. Mahmood, N. H. Nasr, and K. A. Elraies, Foam flow in porous media: Concepts, models and challenges, J. Nat. Gas Sci. Eng. **53**, 163 (2018).
[29] G. J. Hirasaki and J. B. Lawson, *Mechanisms of Foam Flow in Porous Media: Apparent Viscosity in Smooth Capillaries* (Society of Petroleum Engineers, 1985).
[30] F. P. Bretherton, The motion of long bubbles in tubes, J. Fluid Mech. **10**, 166 (1961).
[31] H. Soo and C. J. Radke, A filtration model for the flow of dilute, stable emulsions in porous media—I. Theory, Chem. Eng. Sci. **41**, 263 (1986).
[32] D. Bartolo, G. Degré, P. Nghe, and V. Studer, Microfluidic stickers, Lab Chip **8**, 274 (2008).
[33] B. Levaché, A. Azioune, M. Bourrel, V. Studer, and D. Bartolo, Engineering the surface properties of microfluidic stickers, Lab Chip **12**, 3028 (2012).
[34] M. Romano, M. Chabert, A. Cuenca, and H. Bodiguel, Strong influence of geometrical heterogeneity on drainage in porous media, Phys. Rev. E **84**,065302(R) (2011).
[35] See Supplemental Material at http://link.aps.org/supplemental/10.1103/PhysRevFluids.5.094004 for more details on micromodel fabrication, the foam injection method, the image analysis method, characterization of a bubble train, and the full preferential path cartography.
[36] S. Ayatollahi and A. Rabbani, Comparing three image processing algorithms to estimate the grain-size distribution of porous rocks from binary 2D images and sensitivity analysis of the grain overlapping degree, Spec. Top. Rev. Porous Media **6**, 71 (2015).
[37] M. Chen, Y. C. Yortsos, and W. R. Rossen, Insights on foam generation in porous media from pore-network studies, Colloids Surf. A **256**, 181 (2005).
[38] S. Kahrobaei, S. Vincent-Bonnieu, and R. Farajzadeh, Experimental study of hysteresis behavior of foam generation in porous media, Sci. Rep. **7**, 8986 (2017).
[39] O. Fergui, H. Bertin, and M. Quintard, Transient aqueous foam flow in porous media: Experiments and modeling, J. Petrol. Sci. Eng. **20**, 9 (1998).
[40] O. Gassara, F. Douarche, B. Braconnier, and B. Bourbiaux, Equivalence between semi-empirical and population-balance foam models, Transp. Porous Media **120**, 473 (2017).
[41] W. L. Olbricht and L. G. Leal, The creeping motion of immiscible drops through a converging/diverging tube, J. Fluid Mech. **134**, 329 (1983).
[42] P. A. Gauglitz and C. J. Radke, Dynamics of Haines jumps for compressible bubbles in constricted capillaries, AIChE J. **35**, 230 (1989).
[43] Q. Xu and W. R. Rossen, Effective viscosity of foam in periodically constricted tubes, Colloids Surf. A **216**, 175 (2003).
[44] S. L. Anna, N. Bontoux, and H. A. Stone, Formation of dispersions using "flow focusing" in microchannels, Appl. Phys. Lett. **82**, 364 (2003).
[45] N. A. Mortensen, F. Okkels, and H. Bruusl, Reexamination of Hagen-Poiseuille flow: Shape dependence of the hydraulic resistance in microchannels, Phys. Rev. E **71**, 057301 (2005).
[46] S. Sinha, A. Hansen, D. Bedeaux, and S. Kjelstrup, Effective rheology of bubbles moving in a capillary tube, Phys. Rev. E **87**, 025001 (2013).